

Article

Study on Modified Liquid Polysulfide Rubber Bimetallic Salt-Spray-Resistant Epoxy Coatings

Qitong Mao¹, Siqu Liu¹, Hao Jiang¹, Hua Sun², Yangkai Xiong¹, Zhiqiang Fang¹, Jiang Li³
and Guoqing Wang^{1,*}

¹ State Key Laboratory of Marine Resource Utilization in South China Sea, School of Materials Science and Engineering, Hainan University, Haikou 570228, China

² Shanghai Chemical Industrial Park Pipe Gallery Company, Shanghai 200000, China

³ Industrial & Manufacturing Engineering, College of Engineering, Florida State University, Tallahassee, FL 32306, USA

* Correspondence: wangguoqing@hainanu.edu.cn

Abstract: In this study, liquid polysulfide rubber was modified by silane coupling agent. New kinds of anti-corrosion coatings with salt spray resistance and strong adhesion to the steel substrate were obtained using the modified liquid polysulfide rubber, bimetallic filler, carbon nanotubes, and epoxy resin. Infrared and nuclear magnetic resonance confirmed the preparation of new modified liquid polysulfide rubber through coupling reaction between the epoxy group of silane compound and the sulfide group of the liquid polysulfide rubber. A 1440 h neutral salt spray test showed the coating to be completely free of rust and blisters. The corrosion diffusion width of the scribed area was only 1.7 mm. In addition, in a 3.5% by weight NaCl solution, the coating shows no blistering and no corrosion phenomena compared with zinc-rich epoxy paints (the added zinc content was only 28.6%). These tests confirmed that the new coating had a dense microstructure, strong adhesion to the steel substrate, good corrosion resistance, and anti-blister performance. The performance indicates that the coatings have potential for use in the atmosphere and underwater, which provides a better choice for long-term protection of marine projects such as ships, wharves, offshore platforms, and wind power structures.

Keywords: modified epoxy coatings; modified liquid polysulfide rubber; bimetallic anti-corrosion; underwater protection; long-term heavy-duty anti-corrosion; low zinc content



Citation: Mao, Q.; Liu, S.; Jiang, H.; Sun, H.; Xiong, Y.; Fang, Z.; Li, J.; Wang, G. Study on Modified Liquid Polysulfide Rubber Bimetallic Salt-Spray-Resistant Epoxy Coatings. *Coatings* **2022**, *12*, 1418. <https://doi.org/10.3390/coatings12101418>

Academic Editor: Edoardo Proverbio

Received: 19 August 2022

Accepted: 20 September 2022

Published: 27 September 2022

Publisher's Note: MDPI stays neutral with regard to jurisdictional claims in published maps and institutional affiliations.



Copyright: © 2022 by the authors. Licensee MDPI, Basel, Switzerland. This article is an open access article distributed under the terms and conditions of the Creative Commons Attribution (CC BY) license (<https://creativecommons.org/licenses/by/4.0/>).

1. Introduction

In the 21st century, with the problem of the misuse of natural resources due to the explosive population growth, there is a shortage of resources on land that urgently needs to be solved. The ocean makes up 71% of the total area of the earth. The rich mineral and biological resources of the ocean are gifts from nature to man, and their exploitation is the key to solving the harmonious coexistence between man and nature [1–4].

In the development of the ocean, we have to resort to various oceanic projects. Steel materials are widely used in the construction of ships, sea crossing bridges, offshore platforms, offshore wind power, offshore terminals, and other industries because of their high strength, easy processing, and recyclability. However, steel corrodes easily in humid environments [5–10]. Zinc-rich epoxy coatings have been widely used since the 1980s due to their excellent anti-corrosion properties [11–13]. Epoxy zinc-rich paint is a widely used anti-rust primer, but its brittleness and high zinc content (the content of metallic zinc in the coating shall not be less than 60% in HG/T3668) is not suitable for underwater environments. In high humidity and a hot atmosphere, the coating blisters very easily. Therefore, it is urgent to find suitable coatings for long-term use in the underwater environment [14,15].

An epoxy high performance anti-corrosion coating has the advantages of strong corrosion resistance [16,17], high hardness, good adhesion, etc. It can be mixed with

a variety of fillers and anti-corrosion additives [18–21]. However, the traditional epoxy resin coatings have a high content of volatile organic compounds [22]. High brittleness, poor post-cure weatherability, and poor adhesion limited their wider application. Most epoxy zinc-rich coatings on the market are usually used as primers. If used alone, epoxy zinc-rich coatings were brittle and not suitable for long-term corrosion protection. In addition, they tend to form blisters on the paint surface, which limits their industrial applicability. Currently, there is a lot of research on the possibility of reducing the zinc content in soil [23]; in this experiment, we want to explore a corrosion-resistant epoxy coating with low zinc content that can be used in both atmospheric and underwater environments.

The main chain of liquid polysulfide rubber contains sulfur atoms and saturated-bonds -S-C- or -S-S-. The sulfide bond can be moved; thus, the whole molecular chain has good flexibility. After the sulfide group(-SH) contained at the end of the molecule reacts with the epoxy ring group of the silane coupling agent, the end of the molecular chain contains the silane group. The silane group can react with the moisture on the surface of the metal powder to form siloxane [24,25], and the other end can be combined with organic substances to form a molecular bridge between the organic and inorganic structures to ensure the bond of increasing strength [26–29].

Titanium has the characteristics of non-toxicity, low density, high specific strength, and low electrode potential. It is suitable for use as a coating additive [30] with good corrosion resistance [31,32]. Furthermore, zinc metal has the characteristics of strong activity, taking the lead into protection against substrate corrosion, filling the coating pores with products after corrosion, and continuously providing protection for subsequent service [33]. Therefore, titanium metal and zinc metal can improve the compactness of the coatings at different stages.

In this experiment, the new coating was made by high-energy ball milling to grind epoxy resin [34–36], modified liquid polysulfide rubber, titanium metal, zinc metal, and other fillers under N₂. The good corrosion resistance of the coating can reduce corrosion products, increase the corrosion resistance to aging, and make the coating work underwater. This study is expected to provide a long-term anti-corrosion coating with low zinc content and can be used both in the atmosphere and underwater, providing a new choice for long-term protection of marine engineering and reducing the use of metallic zinc.

2. Materials and Methods

2.1. Materials

Liquid polysulfide rubber, Epoxy Resin 0164, Zinc powder, and Q235 Steel Plate (Sand-blasted) were purchased from Shanghai Sunvea Chemical Material Technology Co., Ltd. (Shanghai, China). Silane coupling agent was obtained commercially through Sinopharm Chemical Reagent Co., Ltd. (Shanghai, China). Xylene, butyl acetate, and petroleum ether were purchased from Guangdong Guanghua Technology Co., Ltd. (Shantou, China). Titanium powder, carbon nanotubes, and polyamide curing agent 650 were purchased from Jiangsu Sanmu Chemical Co., Ltd. (Wuxi, China).

2.2. Method

2.2.1. Preparation of Modified Liquid Polysulfide Rubber

The liquid polysulfide rubber was mixed with a silane coupling agent and xylene with a weight ratio of 1.7:1:3.2 in a three-neck flask. After 30 h at 120 °C with nitrogen gas, a transparent viscous liquid product was obtained. Then, the mixture was put in a partition funnel and extracted twice by an equal volume of petroleum ether. Finally, the modified liquid polysulfide rubber was obtained by collecting the viscous underlayer [37].

2.2.2. Preparation of the Coatings

As shown in Figure 1, modified polysulfide liquid rubber, epoxy resin, titanium powder, zinc powder, and carbon nanotubes were added to the pot in different proportions to prepare the epoxy resin composite coating. The rotation of the high-speed ball mill was per-

formed at high speed under nitrogen atmosphere for 10 h; MPSR coatings including MPSR0 ($m_{EP}:m_{Ti} = 1:1$), MPSR1 ($m_{EP}:m_{MPSR}:m_{Ti} = 2:1:2$), MPSR2 ($m_{EP}:m_{MPSR}:m_{Ti}:m_{Zn} = 2:1:2:2$), MPSR3 ($m_{EP}:m_{MPSR}:m_{Ti}:m_{CNTs} = 2:1:2:0.06$) and MPSR4 ($m_{EP}:m_{MPSR}:m_{Ti}:m_{Zn}:m_{CNTs} = 2:1:2:2:0.06$), were prepared by changing the ratio of fillers. A certain amount of Polyamide Curing Agent 650 and a small amount of a mixed solvent of xylene and butyl acetate were added to each of the five coatings. After sandblasting (cleanliness: ISO 8501-1 Sa2 $\frac{1}{2}$), they were evenly brushed on the Q235 steel plate and stored at room temperature for 7 days. Additionally, the target coatings were able to be obtained.

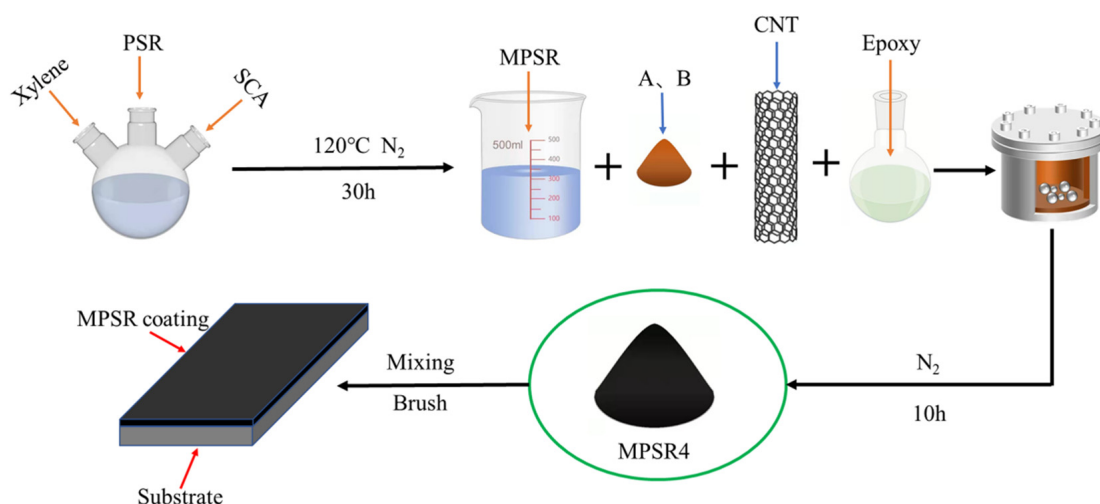


Figure 1. Preparation of modified polysulfide rubber epoxy coating.

2.3. Characterization

2.3.1. Characterization of Modified Liquid Polysulfide Rubber

To confirm the successful production of the modified polysulfide liquid rubber, the changes in the functional groups of the modified polysulfide liquid rubber were examined using Fourier-transform infrared spectroscopy (FT-IR, Bruker, Karlsruhe, Germany) and the spectra were recorded in the range of 4000–400 cm^{-1} . Nuclear magnetic resonance spectroscopy was also performed to characterize the modified polysulfide liquid rubber.

2.3.2. Characterization of the Coatings Layer

The cross-sectional morphology of the coatings was observed on a field emission scanning electron microscope (Gemini SEM 300, Shenzhen, China).

The weight gain rate of the coatings was measured on an electronic balance.

The electrochemical properties of these samples when immersed in a 3.5 wt% NaCl solution were analyzed using a DH7000 (Saiao, Hangzhou, China). The effect of variations in corrosion potential on the coating was determined by an open-circuit potential (OCP) test, whereas the corrosion resistance of the coatings was characterized by an EIS test with an operating frequency range of 10^{-2} to 10^5 Hz at an amplitude of 10 mV. DHElecChem (version 6.20.42) was used to record and analyze the Nyquist and Bode plots obtained from the tests. Finally, the coatings were tested for polarization curves with a scan voltage in the range of ± 0.25 V (relative to the OCP) and a scan rate of 1 mV/s [38].

The corrosion resistance of the coatings could be demonstrated intuitively using the salt spray test. A sharp tool was used to make a scratch on the board surface across the coating film to expose the underlying metal. The corrosion resistance of the coatings was tested on a salt spray chamber. All samples were measured in an environment of 5 ± 0.5 wt.% NaCl solution environment.

The adhesion of the coatings was measured using the pull-off method according to ASTM D4541-2009 with a PosiTest pull-off adhesion tester (DeFelsko Inc. Ogdensburg, NY, USA). The drawing method was used to measure the adhesion of the coating. An

aluminum forging die with a diameter of 20 mm was glued to the coating, and a pull-off test was carried out after curing for 48 h.

The prepared coating was immersed in a 3.5% NaCl solution and allowed to stand for 60 days to observe the surface state of the plate and the products in the solution. After shaking the solution evenly, 10 mL of the solution was removed for centrifugation, and the centrifuged product was weighed (>0.001 g) on an electronic balance.

3. Results and Discussion

3.1. Characterization of Modified Liquid Polysulfide Rubber

The preparation of the modified liquid polysulfide rubber was shown in Figure 2. The subsequent characterization was performed using FT-IR. Figure 3 shows the FT-IR spectra of modified polysulfide liquid rubber, unmodified polysulfide liquid rubber, and silane coupling agent, respectively. The absorption peak at 2560 cm^{-1} , ascribed to -SH , was observed for the modified liquid polysulfide rubber and liquid polysulfide rubber. Additionally, the absorption peak at 1076 cm^{-1} , coming from -C-O-C- in the modified liquid polysulfide rubber, highly overlapped with that of silane coupling agent at 1088 cm^{-1} . Due to the grafting reaction between the epoxy group on the silane coupling agent and -SH on the PSR, the absorption peaks of the epoxy ring at 910 cm^{-1} and 1255 cm^{-1} , resulting from the epoxy ring on the SCA sample were not found in the spectra of MPSR and PSR. In addition, the absorption peak of the modified polysulfide liquid rubber at 821 cm^{-1} was the same as that of the silane coupling agent. The results mentioned above suggested the successful manufacture of the modified polysulfide liquid rubber.

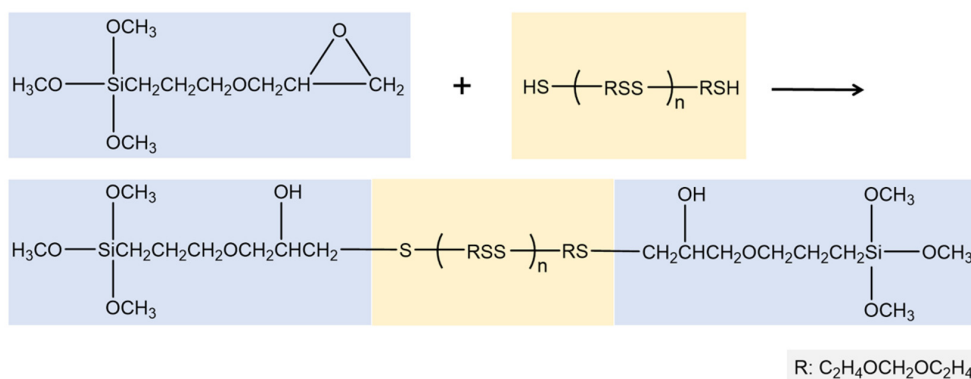


Figure 2. Preparation equation of modified liquid polysulfide rubber.

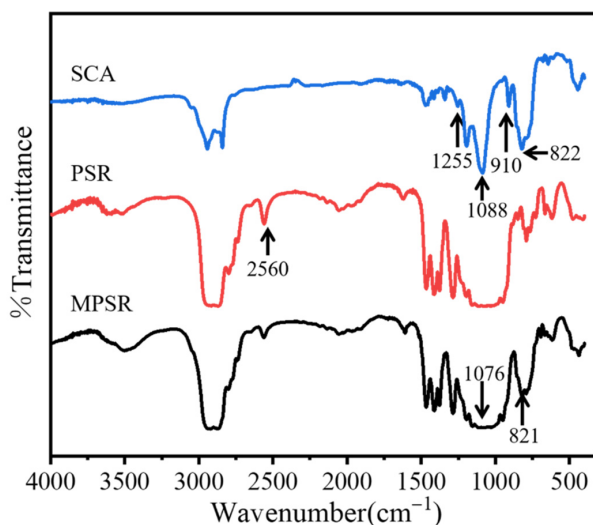


Figure 3. Infrared spectra of MPSR, PSR, SCA.

Further NMR was performed to clarify the MPSR structure. As shown in Figure 4, the signal of the main chain group $-C_2H_4OCH_2OC_2H_4-$ at b in Figure 4a and the proton peak of $-CH_2-$ and $-CH-$ at d in Figure 4a matched, indicating a similar main chain structure exists in SCA, PSR and MPSR. In addition, the position at c in Figure 4a, which corresponds to $-Si(OCH_3)$, matched f in Figure 4c. Additionally, the new peak at a in Figure 4a was assigned to the $-OH$ peak in MPSR arising from the nucleophilic substitution reaction between the epoxy group of SCA and the $-SH$ of PSR. NMR results, consistent with FT-IR, suggested that MPSR was successfully prepared.

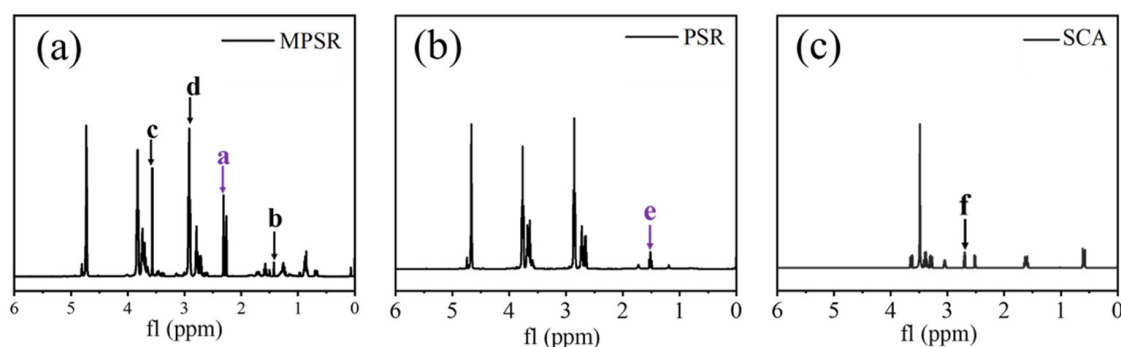


Figure 4. (a) the NMR of SCA; (b) the NMR of PSR; (c) the NMR of MPSR.

3.2. Characterization of Coatings

3.2.1. Section Morphology of the Coatings

Figure 5 shows the cross-sectional scans of the 5 coatings. The 2K SEM image showed that the compactness of MPSR0 is better due to the relatively high proportion of epoxy resin in the coating. Titanium powder was added to the MPSR1, which could be densely filled in the epoxy resin coatings with good compactness. The compactness of MPSR2 was the worst and the apparent pores were evident in Figure 5e. This resulted from the reduction in epoxy in the coating with the addition of metal Ti and metal Zn. In addition, MPSR3 and MPSR4 carbon nanotubes were added as fillers. An interwoven network structure derived from the one-dimensional tubular structure of carbon nanotubes can be formed in the coating, reducing internal pores and improving the compactness of the coatings.

3.2.2. The Weight Gain Rate of the Coatings

From the SEM photos of the coatings, it can be seen that the coatings produced after ball milling have quite good compactness. To better compare the effects of different fillers on the compactness of the coatings, some coating fragments were soaked in deionized water. The weight of the coatings was recorded after 7 days, 14 days and 30 days, respectively. The rate of increase in coating weight was calculated as shown in Figure 6. Epoxy resin content was highest in MPSR0 coatings. The rate of weight gain of the coating containing titanium powder was the slowest and changed little, which was attributed to the dense amount of titanium in the interstices of the coatings. In addition, the addition of modified polysulfide liquid rubber to MPSR1 improved the flexibility of the coatings while reducing epoxy resin content. For example, the rate of weight gain of the MPSR1 coating was lower in the MPSR2 coatings, the addition of zinc powder reduced the epoxy resin content and weakened the compactness of the coatings. In addition, zinc powder, which has the lower potential, acted as a sacrificial anode in the coatings to protect the cathode. Accordingly, the generated zinc oxide and other products filled in the gaps in the coatings, giving the MPSR2 coating the highest rate of weight gain. Carbon nanotubes were introduced for the MPSR3 coating. Since the carbon nanotube content was very low, the epoxy resin content increased; thus, the compactness of MPSR3 coatings was stronger than that of MPSR2, whereas the weight gain rate decreased. As all of the fillers were added to MPSR4, the proportion of zinc powder and epoxy resin decreased. Therefore, the coatings were more

compact than MPSR2 and less compact than MPSR3, and the rate of coating weight gain increased slightly compared with MPSR3.

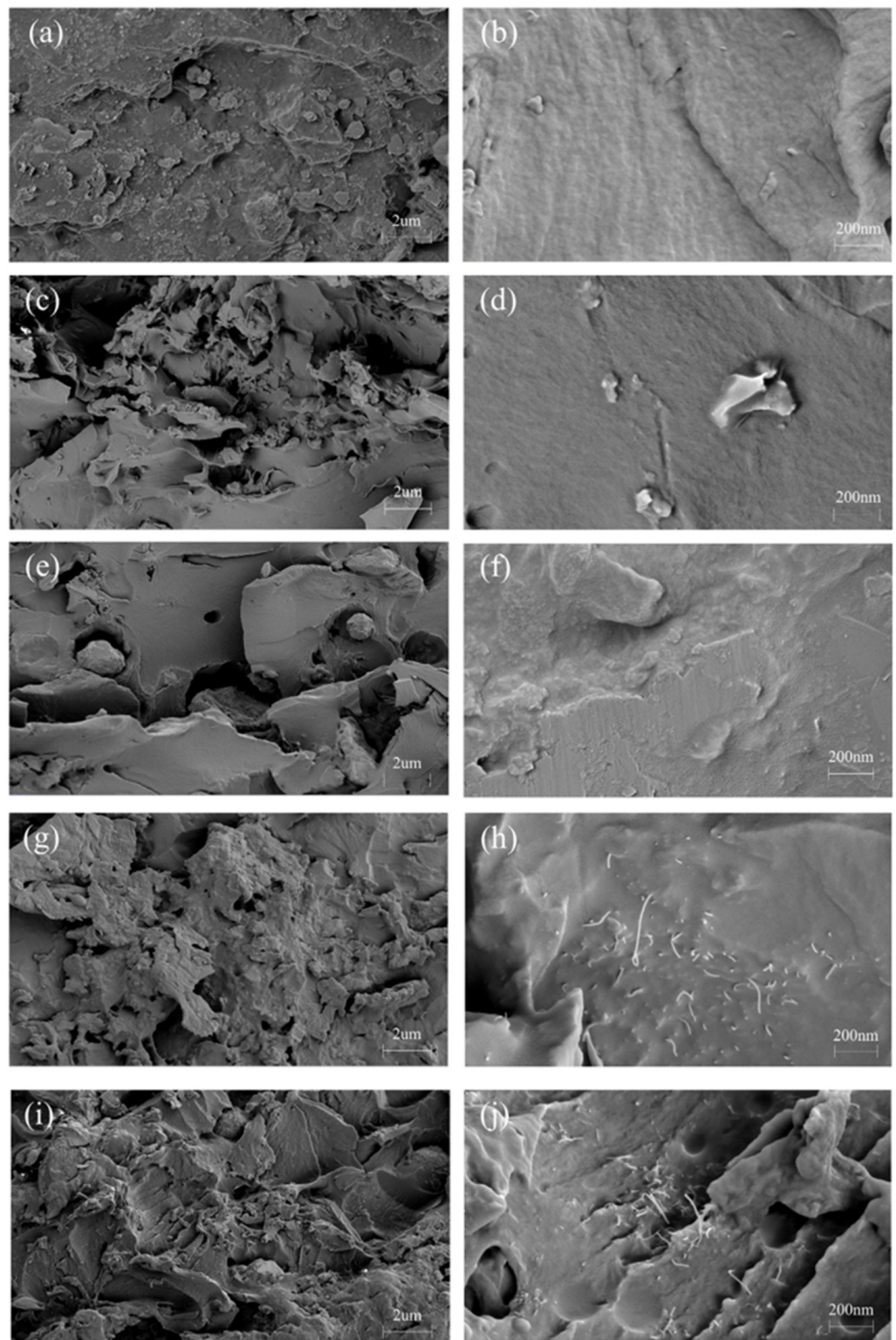


Figure 5. (a) SEM; (b) MPSR0; (c,d) MPSR1; (e,f) MPSR2; (g,h) MPSR3; (i,j) MPSR4.

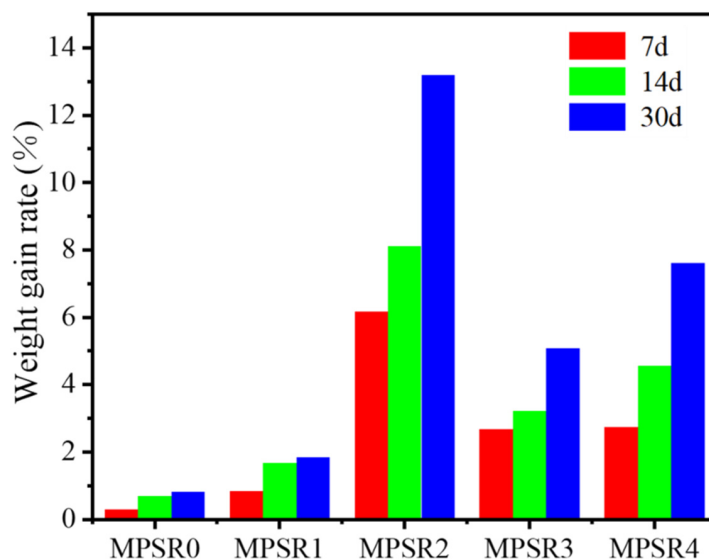


Figure 6. Weight gain rate of coatings.

3.2.3. Characterization of Electrochemistry

In a 3.5 wt% NaCl solution, tafel polarization curves were recorded for the coatings MPSR0, MPSR1, MPSR2, MPSR3, and MPSR4 to examine the corrosion resistance of the coatings. Figure 7 showed the polarization curve of the coatings. Corrosion current (i_{corr}) and corrosion potential (E_{corr}) were obtained by the Tafel extrapolation method, and the corresponding values were shown in Table 1. According to Figure 7 and Table 1, E_{corr} of MPSR1 is the most negative, whereas i_{corr} of the MPSR4 sample was the largest. Additionally, the three samples, MPSR2, MPSR3 and MPSR4 to which zinc powder and carbon nanotubes were added had larger corrosion potentials, of which MPSR2 had the largest corrosion potential. In addition, as can be seen from Table 1, the corrosion current of MPSR0 was the smallest, yet the corrosion potential was only slightly greater than that of MPSR1. This suggested the worst corrosion resistance of MPSR0. The excessive amount of titanium powder in the coating tended to agglomerate and reduced corrosion resistance. This was also proven in the subsequent salt spray test. Based on the analysis mentioned above, the MPSR2 sample had the best corrosion resistance.

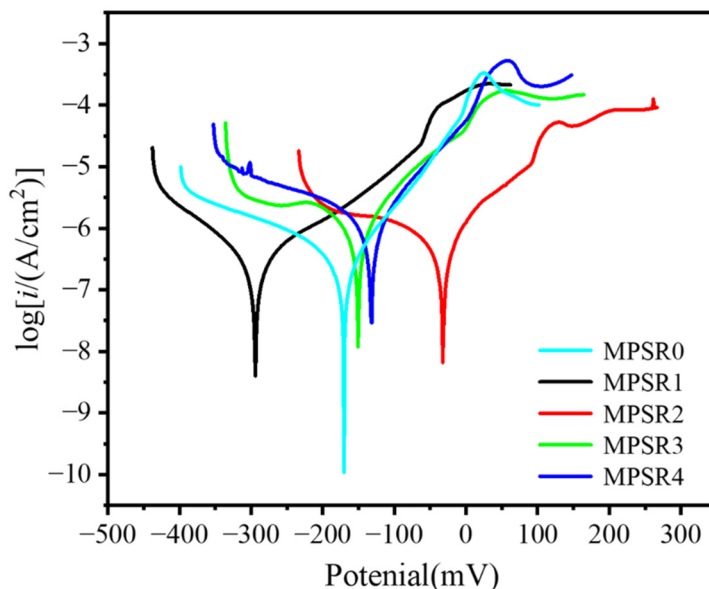


Figure 7. Tafel polarization curve for the coatings.

Table 1. Corrosion current and corrosion potential of five kinds of coating samples.

Sample	$i_{\text{cor}} 10^{-6} \text{ (A/cm}^2\text{)}$	$E_{\text{cor}} \text{ (mV)}$
MPSR0	0.08059	−168.9
MPSR1	0.1006	−295.7
MPSR2	0.1669	−27.40
MPSR3	0.2788	−147.7
MPSR4	0.5177	−125.3

Electrochemical impedance tests were performed on five samples with similar coating thicknesses. The coated steel block, with an exposed area of about 1 cm^2 , was the working electrode, and the saturated calomel electrode was chosen as the reference electrode, whereas the platinum electrode was the counter electrode. The EIS test was carried out after the working electrode was immersed in a 3.5% NaCl solution. Figure 8 illustrated the Bode plot of the EIS test for the coated electrodes of MPSR0, MPSR1, MPSR2, MPSR3, and MPSR4 from 360 h to 720 h. Under normal circumstances, the corrosion resistance of the coating could be evaluated by the value of the impedance modulus in the low-frequency range of the Bode diagram. The larger the value of the impedance modulus in the low frequency range, the better the corrosion resistance. With increasing dive time, the impedance in the low-frequency range decreased. In addition, the impedance modulus of MPSR2 was two orders of magnitude greater than that of the other four coatings. This showed that the corrosion resistance of MPSR2 was the best. This may be the combined impact of the serious effect on the addition of titanium powder and the protection of the cathode by the sacrificial anode after the addition of zinc powder. In addition, among the other four samples, the value of the impedance modulus of the MPSR sample was largest in the low frequency range, which could confirm the results of the salt spray test. Compared with MPSR2, the smaller value of the impedance modulus of MPSR1 in the low frequency range indicated the anti-corrosion effect of zinc powder. However, the value of the impedance modulus of the MPSR4 sample containing zinc powder was smaller. The simultaneous incorporation of zinc powder and carbon nanotubes into MPSR4 reduced the epoxy resin content and thus weakened the compactness of the coating. Additionally, the special one-dimensional structure of carbon nanotubes led to the contact between the coatings and the corrosive medium and reduced the anti-corrosion performance.

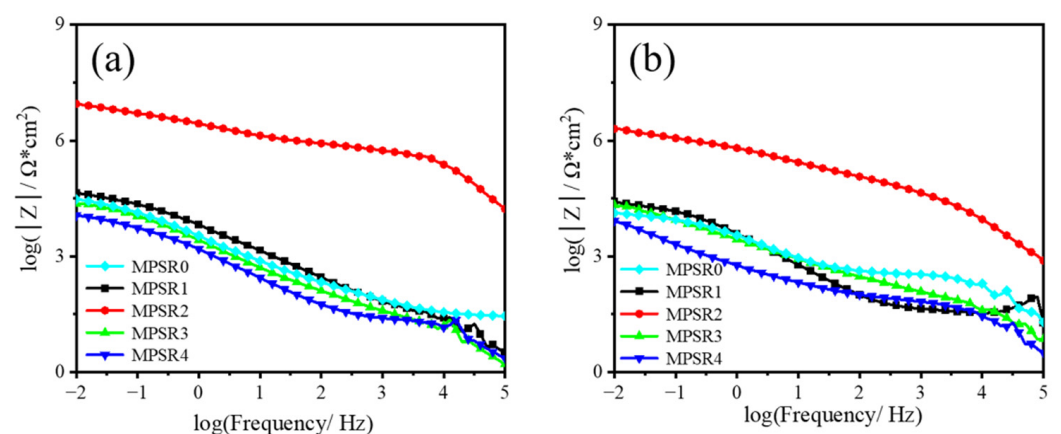
**Figure 8.** (a) Bode diagram of 360 h for 5 kinds of coatings; (b) Bode Diagram of 720 h for 5 kinds of coatings.

Figure 9 shows the Nyquist plots of MPSR0, MPSR1, MPSR2, MPSR3, and MPSR4 samples at 720 h. In general, the trend in changes of the 5 samples with increasing immersion time was similar to the increase in immersion time, and they all showed monoclonal antibodies. Among them, the MPSR2 sample had the largest radius with only one time constant. This showed the nature of pure capacitance and has good protection performance

of the MPSR2 sample. Although the other samples had only one time constant, the smaller radius of the capacitive reactance arc caused its weaker protection performance. With the exception of MPSR2, the MPSR1 sample had the largest capacitive reactance arc radius, followed by r_{MPSR4} , r_{MPSR3} , and r_{MPSR0} . This agreed with the corrosion resistance capacity, which was confirmed by the salt spray experiment.

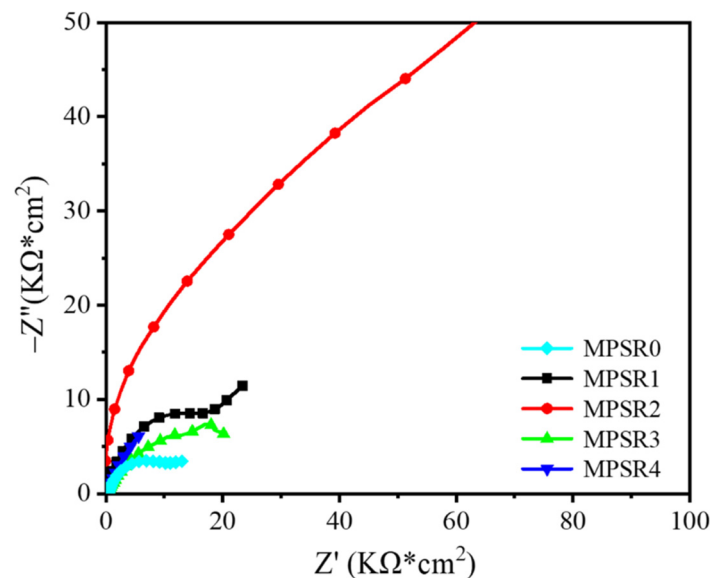
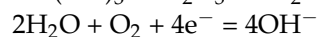


Figure 9. Nyquist plot of MPSR0, MPSR1, MPSR2, MPSR3, MPSR4 samples after 720 h.

3.2.4. Characterization of Coating Salt Spray Test

Figure 10 shows the photos of the salt spray test of 5 kinds of coatings at different times (0 h, 360 h, 720 h, 1440 h). The MPSR0 sample had blistered at 360 h and 720 h, and the phenomenon has spread across the board. At the same time, the corrosion on the scratches was extremely severe. This was because Fe is more active than titanium metal. Throughout the coating system, Fe acted as an anode to exert a protective effect. At this point, the reaction was as follows:



Titanium metal was on the protected side of the entire system at 720 h, and the gas generated could not break through the coatings; thus, bubbles were observed with the naked eye.

At 720 h, no bubbles were found in the MPSR1 sample. However, after 1440 h, a very small number of bubbles were generated. Therefore, the coatings had a positive effect on the spread of corrosion phenomena on the scratches. Compared to the MPSR0 sample, the addition of MPSR introduced the flexible group $-\text{OCH}_3$ to avoid stress concentrations and improve the adhesion of the coatings. After grinding in the ball mill, a corrosion-resistant molecular chain with organic-inorganic structures is created from the titanium powder and the resin molecules through physical-chemical processes. As a filler, titanium powder had excellent passivation and could react with oxygen to form a dense oxide film. Ball milling greatly improved the surface performance of the coating. Further uniform combination of titanium powder with epoxy resin using high speed milling would decrease the surface energy and form the dense network structure which showed good anti-corrosion. This was confirmed by the photos taken by the scanning electron microscope and the EDS test. As corrosion occurred and the corrosive medium penetrated the coatings to reach the substrate, the titanium powder evenly filled the micropores into the coatings. Additionally, the labyrinth effect, namely the distance between the coatings and the substrate, improved

the adhesion of the coatings and thus significantly increased the anti-corrosion performance of the coatings.

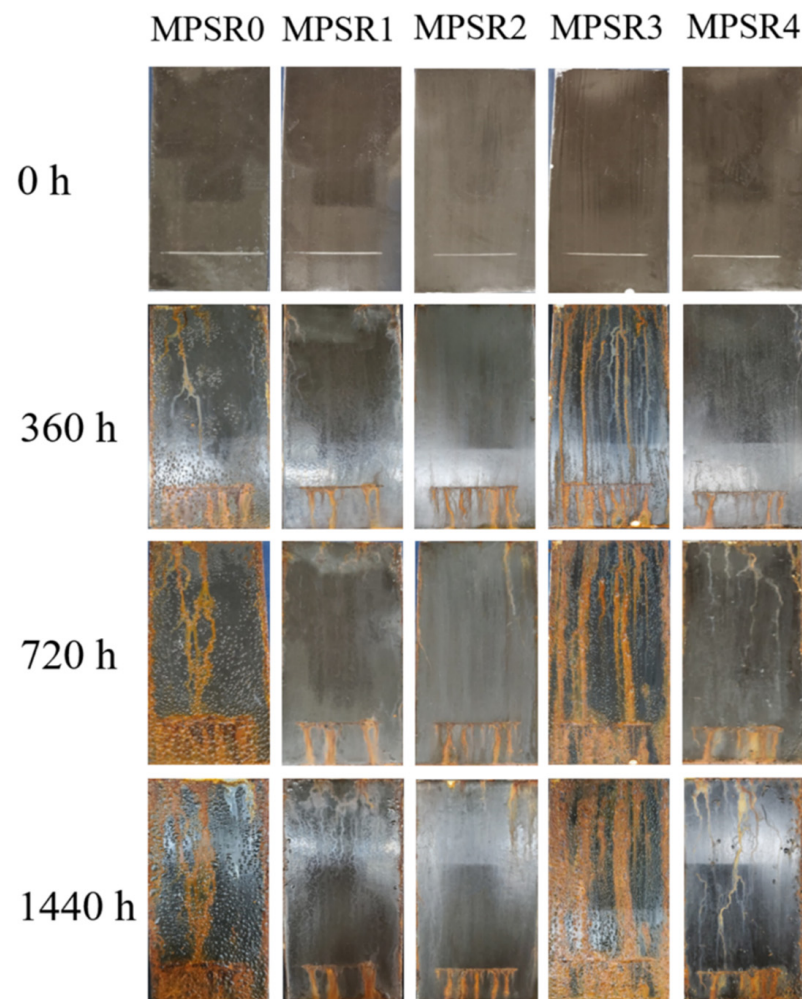
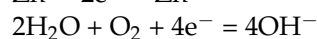
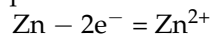


Figure 10. Salt spray test of MPSR0, MPSR 1, MPSR 2, MPSR 3 and MPSR 4 after 0 h, 360 h, 720 h, and 1440 h, respectively.

No surface blisters were observed on the MPSR2 sample after 1440 h. Therefore, the anti-corrosion effect by propagation at the scratches was more significant than that of MPSR1. This could be attributed to the higher activity of Zn than Fe and Ti. In the system, zinc powder as the sacrificial anode protected the Fe as the cathode. The reaction was then:



At the same time, the insoluble $\text{Zn}(\text{OH})_2$ film formed by anodic reaction and the formation of chloride deposited on the coating promoted the passivation of Zn and prevented the corrosive medium from contacting the substrate. With the synergistic effect of titanium powder, good anti-corrosion performance occurred in MPSR2. Figure 11 shows Atomic Force Micrographs of MPSR2 coatings before and after the salt spray test. After the salt spray test, the coating surface obviously changed from flat to rough. EDS analysis showed that titanium powder and zinc powder are evenly distributed in the coatings. During the continuous adsorption of Cl^- in the salt spray test, the oxide film of Ti and Zn partially or completely dissolved, and the corresponding chloride formed at the adsorption site. In addition, due to the uniform distribution of Ti and Zn in MPSR2 coatings, the coatings gradually formed an inverted pyramid structure under the corrosion of chloride ions. When the passivation film of the upper surface coating is eroded, Ti and Zn quickly form

a new passivation film containing chloride, which improves its anti-corrosion property. Under the synergistic effect of such layer-by-layer-like inverted pyramid structure, the corrosion resistance of MPSR2 coatings was particularly excellent.

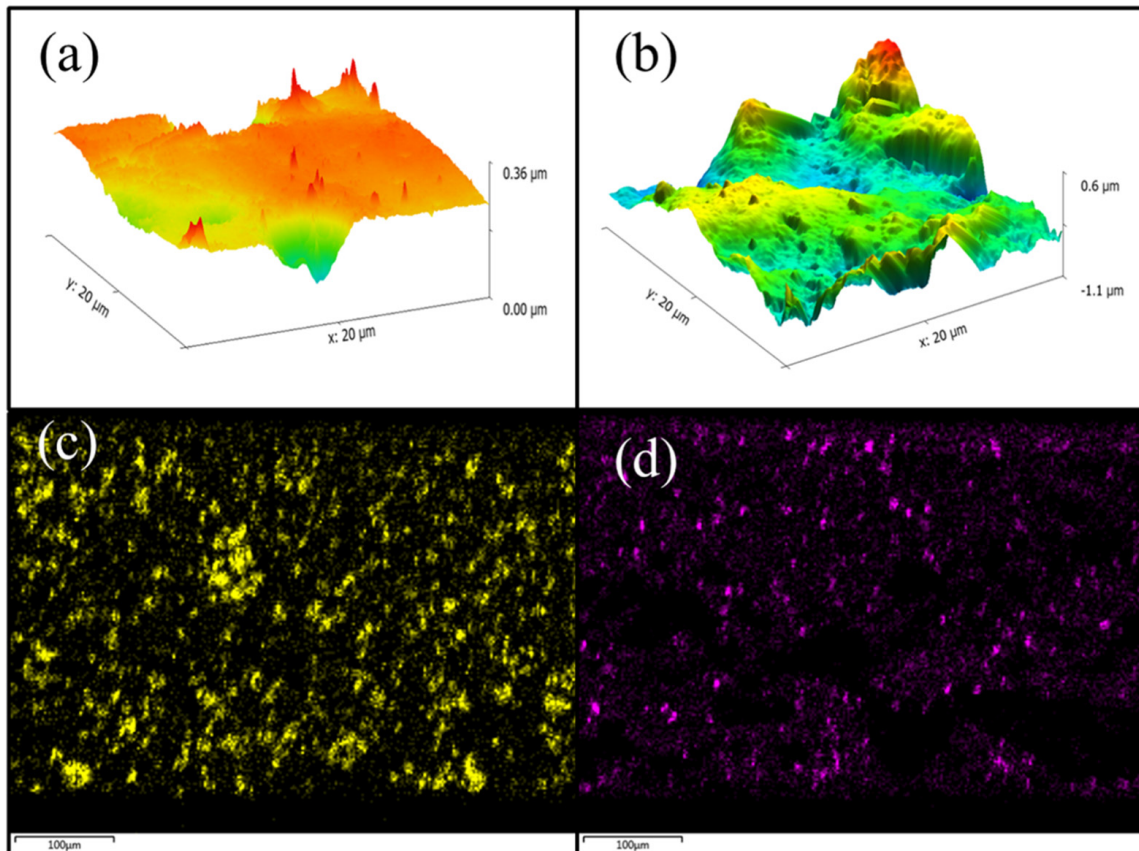


Figure 11. (a) MPSR 2 before corrosion; (b) after MPSR2 corrosion; (c) EDS of MPSR 2 section Ti; (d) EDS of MPSR 2 section Zn.

In Figure 10, many bubbles appeared on the surface of the MPSR3 sample after 360 h. After 720 h, it covered more and after 1440 h almost the entire board. These indicated the serious corrosion phenomenon. However, the scratches were still observed. Compared to the MPSR0 sample, MPSR3 showed a slightly better anti-corrosion effect. According to the electron micrograph conducted 20,000 times, carbon nanotubes with special tube structures somewhat improved the compactness of the coatings while increasing the contact area with the salt spray gas. As a result, a large amount of blistering was found, and the anti-corrosion effect of MPSR3 was not good.

With sample MPSR4, no blistering was observed after 360 h, and the scratches had a good effect of preventing corrosion propagation. However, it was observed at 720 h. Additionally, after 1440 h, the number of blisters on the coating surface did not increase significantly. Zinc powder was added to MPSR4 and compared with MPSR3. Zinc powder as a sacrificial anode had good anti-corrosion effects. However, the addition of carbon nanotubes outweighed the anti-corrosion effect of the zinc powder and resulted in corrosion occurring more quickly. This puts the anti-corrosion effect of MPSR4 coatings in third place behind MPSR1 and MPSR2.

In the salt spray experiment, the surface of the pure epoxy resin coating was covered with bubbles after 168 h and the scribe width reached 8 mm after 30 days. Table 2 shows the diffusion value of 1440 h cracking of the coatings (The initial width is 1.5 mm). The diffusion of single metal modified polysulfide liquid rubber epoxy coatings has been reduced from 7 mm to 2 mm compared to MPSR0 coatings, greatly improving the ability to prevent

corrosion diffusion. In addition, the diffusion of the bimetallic modified polysulfide liquid rubber epoxy coating was 0.3 mm, which was smaller than that of single metal modified polysulfide liquid rubber epoxy coatings. Thus, it showed more excellent performance in preventing corrosion diffusion.

Table 2. The scratch width of the coatings at 1440 h.

Sample	MPSR0	MPSR1	MPSR2	MPSR3	MPSR4
Width	7.0 mm	2.0 mm	1.7 mm	5.0 mm	2.5 mm

The contents of different samples are shown in Table 3 Overall, the MPSR2 sample had the best effect on preventing corrosion diffusion and corrosion, followed by MPSR1, whereas the MPSR0 sample had the worst anti-corrosion performance.

Table 3. Content of different samples.

Sample	EP(g)	MPSR(g)	Ti(g)	Zn(g)	CNTs(g)
MPSR0	20	-	20	-	-
MPSR1	20	10	20	-	-
MPSR2	20	10	20	20	-
MPSR3	20	10	20	-	0.6
MPSR4	20	10	20	20	0.6

3.2.5. Adhesion of Coatings

From the salt spray test, we can see the influence of different fillers on the corrosion resistance of the coatings. In order to investigate the influence of different fillers on the mechanical properties of the coatings, the adhesion of the coatings was tested.

The adhesion data of the coatings are shown in Figure 12. MPS R0 had the lowest adhesion, and the MPSR1 had the highest adhesion. After MPSR1 was added to MPSR, the introduction of flexible groups avoided stress concentration and increased the coating adhesion from 6.543 MPa to 9.729 MPa with an increase of 48.7%. The addition of zinc powder to MPSR2 caused the adhesion to deteriorate. Additionally, the introduction of carbon nanotubes into MPSR3 increased the bonding force between the coatings and the metal and improved adhesion. However, due to the increase in pigments in MPSR4, even with the addition of a small amount of carbon nanotubes, the adhesive strength was still reduced.

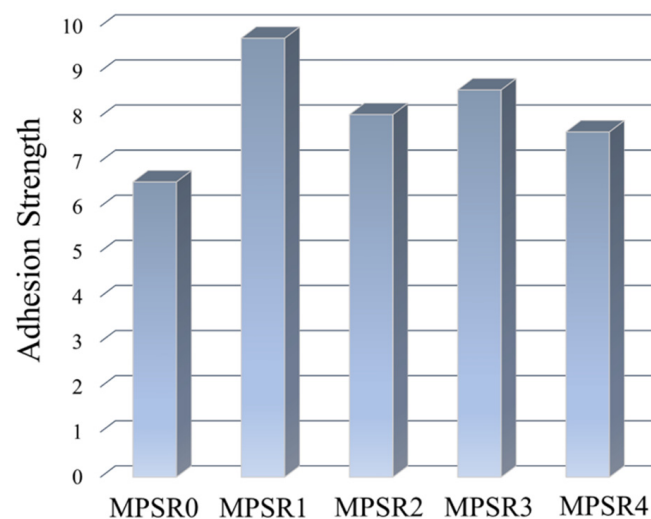


Figure 12. Coating adhesion test.

3.3. Coating Immersion Test

To test whether the coatings have good immersion resistance, the MPSR2 coating with the best anti-corrosion performance and the commercially available polyurethane coating were applied to a panel and placed in a 3.5% NaCl solution. Then, the changes in the coating surface were recorded and observed. As shown in Figure 13a,b, there was no change in the surface of the MPSR2 coatings after 60 days of immersion. In Figure 13c the zinc-rich coatings precipitate a large amount of zinc salts on the surface after immersion, this is normal for zinc-rich coatings and the zinc corrosion products seal the coating and thus provide barrier protection. In the solution dipped in MPSR2 coatings, there was corrosion on the exposed part of the panel. After centrifuging the product in the solution, the product obtained accounts for only 0.5% of the solution. This showed that the MPSR2 coatings had good resistance to water immersion. The mass ratio of added zinc powder is only 28.6%, which greatly reduces the use of metallic zinc.

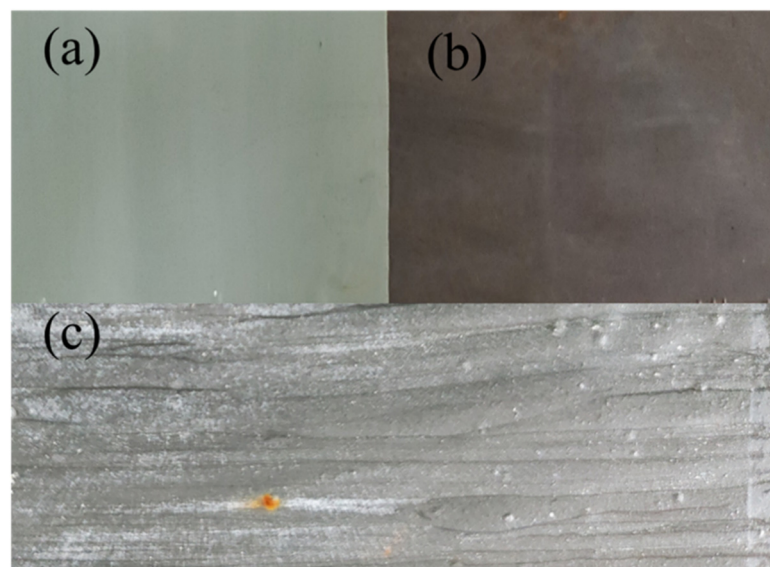


Figure 13. (a) Polyurethane coating; (b) MPSR2; (c) zinc-rich coating.

4. Conclusions

In this study, coatings of MPSR0, MPSR1, MPSR2, MPSR3, and MPSR4 were prepared by adding modified polysulfide liquid rubber, metal-Ti, metal-Zn, and carbon nanotube fillers to epoxy resin. After conducting SEM, weight increase rate, salt spray test, electrochemical test and other experiments on the coating, the results showed:

- (1) The polysulfide liquid rubber is successfully modified by the silane coupling agent. Compared with the epoxy resin coating, the modified polysulfide liquid rubber-epoxy monometallic coating showed better corrosion resistance, and the salt spray foam resistance of the coatings was greatly improved. Blistering time with coatings increased from 72 h to 720 h, and the adhesion of the coatings was greatly improved from 6.543 MPa to 9.729 MPa, with an increase of 48.7%. The corrosion spread of the coating salt spray system has been greatly reduced, from 7.0 mm to 1.7 mm.
- (2) Bimetal combination with different potential parameters (Ti and Zn) could improve the corrosion resistance and blistering resistance of the coatings, and the bimetal epoxy coating could achieve corrosion resistance of 1440 h. As a result, the impedance could be two orders of magnitude higher than that of a single-metal epoxy coating.
- (3) Compared with the single metal epoxy coating, the modified polysulfide liquid rubber bimetal anti-salt spray epoxy coating showed higher impedance, low surface exudation, long-term resistance to saltwater immersion, and no change in the surface of the coating, the added zinc content was only 28.6%. The coating had a high initial

weight gain rate, and a dense long-term protective coating was obtained. It is a long-term anti-corrosion coating that can be used for a long time in both saline atmosphere and underwater environments. It is expected to be widely used in marine engineering.

Author Contributions: Conceptualization, G.W. and Q.M.; methodology, Q.M.; validation, Q.M., S.L. and H.J.; formal analysis, Q.M. and H.S.; investigation, Q.M. and Z.F.; resources, G.W.; data curation, Q.M.; writing—original draft preparation, Q.M. and J.L.; writing—review and editing, G.W.; visualization, Y.X.; supervision, G.W.; project administration, G.W.; funding acquisition, G.W. and H.S. All authors have read and agreed to the published version of the manuscript.

Funding: This research was funded by the National Natural Science Foundation of China (grant number 51963008), Natural Science Foundation of Hainan Province (grant number 520MS015).

Institutional Review Board Statement: Not applicable.

Informed Consent Statement: Not applicable.

Data Availability Statement: Data are contained within the article.

Acknowledgments: I would like to express thanks for the support from the Analysis and Testing Center of Hainan University.

Conflicts of Interest: The authors declare no conflict of interest.

References

1. Hou, B.-R.; Zhang, J.; Duan, J.; Li, Y. Corrosion of thermally sprayed zinc and aluminium coatings in simulated splash and tidal zone conditions. *Corros. Eng. Sci. Technol.* **2003**, *38*, 157–160. [[CrossRef](#)]
2. Schumacher, M. *Sea Water Corrosion Handbook*; Noyes Data: Park Ridge, NJ, USA, 1979.
3. Yang, S.; Lee, K.W.; Lu, C.; Mirville, M.; Parham, A. Adhesion Evaluation of Duplex Paint System for Sustainable Infrastructure. *J. Mater. Civ. Eng.* **2017**, *29*, 04017134. [[CrossRef](#)]
4. Zhang, S.H.; Li, M.X.; Yoon, J.H.; Cho, T.Y.; He, Y.Z.; Lee, C.G. Microstructure and corrosion resistance of Ni-based alloy laser coatings with nanosize CeO₂ addition. *Sci. Technol. Adv. Mater.* **2008**, *9*, 035002. [[CrossRef](#)] [[PubMed](#)]
5. Kim, H.-S.; Jeong, Y.-S.; Dao, D.K.; Kim, I.-T. An approach for evaluating tensile strength of painted steel plates from the surface rusting grade. *Corros. Eng. Sci. Technol.* **2018**, *53*, 510–516. [[CrossRef](#)]
6. Jalili, M.; Rostami, M.; Ramezanzadeh, B. An investigation of the electrochemical action of the epoxy zinc-rich coatings containing surface modified aluminum nanoparticle. *Appl. Surf. Sci.* **2015**, *328*, 95–108. [[CrossRef](#)]
7. Lu, X.; Zuo, Y.; Zhao, X.; Tang, Y. The influence of aluminum tri-polyphosphate on the protective behavior of Mg-rich epoxy coating on AZ91D magnesium alloy. *Electrochim. Acta* **2013**, *93*, 53–64. [[CrossRef](#)]
8. Reedy, M.W.; Eden, T.J.; Potter, J.K.; Wolfe, D.E. Erosion performance and characterization of nanolayer (Ti, Cr) N hard coatings for gas turbine engine compressor blade applications. *Surf. Coat. Technol.* **2011**, *206*, 464–472. [[CrossRef](#)]
9. Luo, X.; Zhong, J.; Zhou, Q.; Du, S.; Yuan, S.; Liu, Y. Cationic Reduced Graphene Oxide as Self-Aligned Nanofiller in the Epoxy Nanocomposite Coating with Excellent Anticorrosive Performance and Its High Antibacterial Activity. *ACS Appl. Mater. Interfaces* **2018**, *10*, 18400–18415. [[CrossRef](#)] [[PubMed](#)]
10. Wen, J.-G.; Geng, W.; Geng, H.-Z.; Zhao, H.; Jing, L.-C.; Yuan, X.-T.; Tian, Y.; Wang, T.; Ning, Y.-J.; Wu, L. Improvement of Corrosion Resistance of Waterborne Polyurethane Coatings by Covalent and Noncovalent Grafted Graphene Oxide Nanosheets. *ACS Omega* **2019**, *4*, 20265–20274. [[CrossRef](#)] [[PubMed](#)]
11. Zhou, S.; Wu, Y.; Zhao, W.; Yu, J.; Jiang, F.; Wu, Y.; Ma, L. Designing reduced graphene oxide/zinc rich epoxy composite coatings for improving the anticorrosion performance of carbon steel substrate. *Mater. Des.* **2019**, *169*, 107694. [[CrossRef](#)]
12. Teng, S.; Gao, Y.; Cao, F.; Kong, D.; Zheng, X.; Ma, X.; Zhi, L. Zinc-reduced graphene oxide for enhanced corrosion protection of zinc-rich epoxy coatings. *Prog. Org. Coat.* **2018**, *123*, 185–189. [[CrossRef](#)]
13. Shirehjini, F.T.; Danaee, I.; Eskandari, H.; Zarei, D. Effect of Nano Clay on Corrosion Protection of Zinc-rich Epoxy Coatings on Steel 37. *J. Mater. Sci. Technol.* **2016**, *32*, 1152–1160. [[CrossRef](#)]
14. Luo, X.; Yin, H.; Ren, J.; Yan, H.; Huang, X.; Yang, D.; He, L. Enhanced mixing of binary droplets induced by capillary pressure. *J. Colloid Interface Sci.* **2019**, *545*, 35–42. [[CrossRef](#)] [[PubMed](#)]
15. Ding, R.; Zheng, Y.; Yu, H.; Li, W.; Wang, X.; Gui, T. Study of water permeation dynamics and anti-corrosion mechanism of graphene/zinc coatings. *J. Alloys Compd.* **2018**, *748*, 481–495. [[CrossRef](#)]
16. Hu, H.; He, Y.; Long, Z.; Zhan, Y. Synergistic effect of functional carbon nanotubes and graphene oxide on the anti-corrosion performance of epoxy coating. *Polym. Adv. Technol.* **2017**, *28*, 754–762. [[CrossRef](#)]
17. Wu, Y.; Zhao, W.; Qiang, Y.; Chen, Z.; Wang, L.; Gao, X.; Fang, Z. π - π interaction between fluorinated reduced graphene oxide and acridinium ionic liquid: Synthesis and anti-corrosion application. *Carbon* **2020**, *159*, 292–302. [[CrossRef](#)]

18. Shen, L.; Li, Y.; Zhao, W.; Miao, L.; Xie, W.; Lu, H.; Wang, K. Corrosion Protection of Graphene-Modified Zinc-Rich Epoxy Coatings in Dilute NaCl Solution. *ACS Appl. Nano Mater.* **2018**, *2*, 180–190. [[CrossRef](#)]
19. Modesti, L.A.; de Vargas, A.S.; Schneider, E.L. Repairing concrete with epoxy adhesives. *Int. J. Adhes. Adhes.* **2020**, *101*, 102645. [[CrossRef](#)]
20. Yeon, J. Deformability of Bisphenol A-Type Epoxy Resin-Based Polymer Concrete with Different Hardeners and Fillers. *Appl. Sci.* **2020**, *10*, 1336. [[CrossRef](#)]
21. Giv, A.N.; Ayatollahi, M.R.; Ghaffari, S.H.; da Silva, L. Effect of reinforcements at different scales on mechanical properties of epoxy adhesives and adhesive joints: A review. *J. Adhes.* **2018**, *94*, 1082–1121. [[CrossRef](#)]
22. Sun, M.; Ma, Z.; Li, A.; Zhu, G.; Zhang, Y. Anticorrosive performance of polyaniline/waterborne epoxy/poly (methylhydrosiloxane) composite coatings. *Prog. Org. Coat.* **2019**, *139*, 105462. [[CrossRef](#)]
23. Zubielewicz, M.; Langer, E.; Królikowska, A.; Komorowski, L.; Wanner, M.; Krawczyk, K.; Aktas, L.; Hilt, M. Concepts of steel protection by coatings with a reduced content of zinc pigments. *Prog. Org. Coat.* **2021**, *161*, 106471. [[CrossRef](#)]
24. Wang, S.; Chia, P.-J.; Chua, L.-L.; Zhao, L.-H.; Png, R.-Q.; Sivaramakrishnan, S.; Zhou, M.; Goh, R.G.-S.; Friend, R.H.; Wee, A.T.-S.; et al. Band-like Transport in Surface-Functionalized Highly Solution-Processable Graphene Nanosheets. *Adv. Mater.* **2008**, *20*, 3440–3446. [[CrossRef](#)]
25. Pourhashem, S.; Vaezi, M.R.; Rashidi, A.; Bagherzadeh, M.R. Distinctive roles of silane coupling agents on the corrosion inhibition performance of graphene oxide in epoxy coatings. *Prog. Org. Coat.* **2017**, *111*, 47–56. [[CrossRef](#)]
26. Matsui, T.; Nakajima, M.; Nonaka, T.; Dokoshi, N. New liquid polysulfide polymer terminated with silyl group. *J. Appl. Polym. Sci.* **2004**, *93*, 2642–2649. [[CrossRef](#)]
27. Kurbangaleeva, A.R.; Kurkin, A.I.; Khakimullin, Y.N. Structure and properties of thiokol sealants modified with organosilanes. *Russ. J. Appl. Chem.* **2012**, *85*, 432–436. [[CrossRef](#)]
28. Liu, B.; Wang, Y. A novel design for water-based modified epoxy coating with anti-corrosive application properties. *Prog. Org. Coat.* **2014**, *77*, 219–224. [[CrossRef](#)]
29. Zhan, Y.; Zhang, J.; Wan, X.; Long, Z.; He, S.; He, Y. Epoxy composites coating with Fe₃O₄ decorated graphene oxide: Modified bio-inspired surface chemistry, synergistic effect and improved anti-corrosion performance. *Appl. Surf. Sci.* **2018**, *436*, 756–767. [[CrossRef](#)]
30. Ovchinnikov, S.; Kalashnikov, M.J.S.; Technology, C. Structure and tribological properties of gradient-layered coatings (Ti, Al, Si, Cr, Mo, S) O, N. *Surf. Coat. Technol.* **2021**, *408*, 126807. [[CrossRef](#)]
31. Jiao, X.; Wang, C.; Gong, Z.; Wang, G.; Sun, H.; Yang, H. Effect of Ti on T15M composite coating fabricated by laser cladding technology. *Surf. Coat. Technol.* **2017**, *325*, 643–649. [[CrossRef](#)]
32. Gao, W.; Zhang, Z.; Zhao, S.; Wang, Y.; Chen, H.; Lin, X. Effect of a small addition of Ti on the Fe-based coating by laser cladding. *Surf. Coat. Technol.* **2016**, *291*, 423–429. [[CrossRef](#)]
33. Ramezanzadeh, B.; Mohamadzadeh Moghadam, M.H.; Shohani, N.; Mahdavian, M. Effects of highly crystalline and conductive polyaniline/graphene oxide composites on the corrosion protection performance of a zinc-rich epoxy coating. *Chem. Eng. J.* **2017**, *320*, 363–375. [[CrossRef](#)]
34. Fatemi, D.J.; Harris, V.G.; Browning, V.M.; Kirkland, J.P. Processing and cation redistribution of MnZn ferrites via high-energy ball milling. *J. Appl. Phys.* **1998**, *83*, 6867–6869. [[CrossRef](#)]
35. Arcos, D.; Valenzuela, R.; Vázquez, M.; Vallet-Regí, M. Chemical Homogeneity of Nanocrystalline Zn–Mn Spinel Ferrites Obtained by High-Energy Ball Milling. *J. Solid State Chem.* **1998**, *141*, 10–16. [[CrossRef](#)]
36. Arcos, D.; Valenzuela, R.; Vázquez, M.; Vallet-Regí, M. Frequency behaviour of Zn–Mn ferrites nanoparticles obtained by high-energy ball milling. *J. Magn. Magn. Mater.* **1999**, *203*, 319–321. [[CrossRef](#)]
37. Yang, F.; Ma, W.; Wang, F. Preparation and Characterization of KH-560 Modified Liquid Polysulfide Rubber. *High Perform. Polym.* **2013**, *29*, 156–159.
38. Fang, Z.; Wang, G.; Xiong, Y.; Li, J.; Yang, Y.; Huang, L.; Wang, P.; Liao, J.; Wang, A. Anti-Corrosion Performance of Polyaniline Coated Basalt Rockwool Wastes/Epoxy Resin Coatings. *Coatings* **2021**, *11*, 463. [[CrossRef](#)]